Applied Catalysis B: Environmental 312 (2022) 121404

Contents lists available at ScienceDirect

Applied Catalysis B: Environmental

journal homepage: www.elsevier.com/locate/apcatb

Molybdenum-based nitrogen carrier for ammonia production via a chemical looping route

Song Yang [a,c,1], Tan Zhang [b,c,1], Yanyan Yang [d], Bixi Wang [a,c], Jin Li [c], Zhouting Gong [a,c], Zhengyue Yao [d], Wenguang Du [b,c], Shoujun Liu [a,c,*], Zhongliang Yu [c,d,*]

[a] College of Chemical Engineering and Technology, Taiyuan University of Technology, Taiyuan 030024, China
[b] Key Laboratory of Coal Science and Technology of Ministry of Education and Shanxi Province, Taiyuan University of Technology, Taiyuan 030024, China
[c] Engineering Center of Civil Clean Fuel, Taiyuan 030024, China
[d] School of chemistry and Environmental Sciences, Shangrao Normal University, Shangrao 334000, China

ARTICLE INFO

Keywords:
Chemical looping ammonia synthesis
Molybdenum-based nitrogen carrier
Ammonia
Nitrogen release
Nitrogen fixation

ABSTRACT

Chemical looping ammonia synthesis (CLAS) is an innovative and effective method for sustainable ammonia generation, in which efficient N release/fixation of nitrogen carriers (NC) is required for successive ammonia production. Herein, we report a two-step CLAS mediated by a Mo_2N-Mo couple and experimentally validate its N fixation and N release steps under mild conditions. In the N-release step, the NH_3 production rate at 450 °C (> 4576 μmol g^{-1} h^{-1}) was three times higher than that obtained via the thermo-catalytic ammonia synthesis route catalyzed by Mo_2N. In the N-fixation step, the introduction of H_2 enhanced the reaction kinetics between Mo and N_2, accelerating NC regeneration. In addition, only a slight deactivation of NC was observed during the 8-cycle stability test. This study confirmed the preliminary feasibility of using Mo_2N as an NC during the CLAS process.

1. Introduction

Ammonia is an important source for producing fertilizers and most N-containing pharmaceuticals [1,2] and is a hydrogen carrier with high energy density, zero carbon emissions, easy liquefaction, and easy storage and transportation. Ammonia has the potential to replace traditional fossil fuels directly as an internal combustion engine fuel [3,4]. Although the industrial route for ammonia production (Haber-Bosch process) is well developed, it is highly energy-intensive owing to its harsh operating conditions [5,6].

To avoid these strict operating requirements, several ammonia synthesis (AS) approaches under mild conditions have been proposed in recent years, such as photon/electron-driven AS [1–8] and chemical looping ammonia synthesis (CLAS) routes. CLAS is an innovative and environmentally friendly low-pressure ammonia synthesis technology that splits the overall ammonia synthesis reaction into sub-reactions facilitated by a nitrogen carrier (NC) [9]. In this process, NC can be viewed as a nitrogen storage medium for activated nitrogen, which can be utilized to discharge and charge nitride lattices. As shown in Fig. 1, NC reacts with H_2 (or H_2O) in ammonia production reactors to generate NH_3; then, the N-depleted NC is regenerated by N_2 (or N_2 with a reducing agent) in the nitridation reactor [9,10], and the regenerated NC is recycled back to the ammonia production reactor for a new reaction cycle. Owing to its compatibility with intermittent operations, CLAS allows the thermodynamic and kinetic properties of each reaction step to be optimized. Additionally, N_2 and hydrogen sources (H_2 or H_2O) were alternately fed into the different reactors, which prevented competitive adsorption on NC.

The NC couple plays a vital role in the CLAS process and can be divided into three categories. In the first, metal nitrides undergo hydrolysis in the ammonia production reactor, producing the desired NH_3 and stable oxide. Hence, the regeneration of metal nitrides requires sacrificial reducing agents in the nitridation reactor, which is energy-consuming. Typical examples of this type of NC couple are AlN-Al_2O_3 [11–13], Mg-Mg_3N_2-MgO [14], Cr-Cr_2N-Cr_2O_3 [15], and Mn_5N_2-MnO [16]. In the second category, the hydride-imide NC couple is applied to mediate CLAS, in which N_2 is reduced by an alkali/alkaline earth hydride to generate an imide [17]. Subsequently, H_2 hydrogenates the imide to form NH_3 and regenerates hydride. Specifically, it has been shown that BaNH catalyzed by Ni in the CLAS process could produce

* Corresponding authors at: Engineering Center of Civil Clean Fuel, Taiyuan 030024, China.
E-mail addresses: 13303460889@163.com (S. Liu), yzh2401@126.com (Z. Yu).
[1] These authors contributed to the work equally and should be regarded as co-first authors.

https://doi.org/10.1016/j.apcatb.2022.121404
Received 22 January 2022; Received in revised form 2 April 2022; Accepted 9 April 2022
Available online 13 April 2022
0926-3373/© 2022 Elsevier B.V. All rights reserved.

NH_3 at 1 bar and 100 °C [18]. However, the synthesis of these NCs is comparatively more difficult [19]. The third category of NC couples is transition/alkaline earth metal nitrides-based NCs [20]. For example, the hydrogenation of $Mn_6N_{2.58}$, Ca_3N_2, and Sr_2N can produce NH_3 with ammonia synthesis rates of 61.53 μmol g^{-1} h^{-1}, 120.81 μmol g^{-1} h^{-1}, and 87.65 μmol g^{-1} h^{-1} at 550 °C, respectively [21]. Unfortunately, ammonia synthesis rates are still unsatisfactory. In summary, NC with facile preparation and high ammonia production efficiency determines the feasibility and competitiveness of CLAS.

Molybdenum nitride (Mo_2N) also has potential as an NC for CLAS. Mo_2N has been widely applied as a catalyst for NH_3 synthesis [22,23]. Mo_2N, as an efficient electrocatalyst to convert N_2 to NH_3, may be depicted via the Mars-van Krevelen mechanism [24,25], where the N vacancy remaining and reverting behaviors are analogous to the N release and N fixation of CLAS. In addition, it has been theoretically proven that Mo_2N has the potential to be an NC when H_2O is used to generate NH_3 [26,27]. This triggered our interest in experimentally exploring the feasibility of Mo_2N as a transition-metal-nitride-based NC in CLAS, generating NH_3 directly with H_2. To the best of our knowledge, this is the first investigation on this topic.

In this study, Mo-based NCs were synthesized through the facile pyrolysis of ammonium molybdate with hexamethylenetramine under an argon gas atmosphere at different temperatures. Subsequently, the N-release and N-fixation performances of Mo-based NCs were investigated, including the hydrogenation of NC by H_2 for NH_3 production and the recovery of NCs from the nitrogen-depleted NC in an N_2/H_2 atmosphere. Finally, the cyclic performance of the Mo-based NCs were evaluated.

2. Experimental

2.1. Preparation of molybdenum-based NCs

The preparation process was as reported previously [28]. Specifically, 3.5 g of $(NH_4)_6Mo_7O_{24}•4H_2O$ (ammonium molybdate, Sinopharm Chemical, 99%) and 4.0 g of $C_6H_{12}N_4$ (hexamethylenetramine, Sinopharm Chemical, 99%) were dissolved by 50 ml of distilled water; then, these two aqueous solutions were mixed, and the precipitate (Mo-HMT) was obtained. After drying at 120 °C overnight, 250 ± 10 mg Mo-HMT was loaded into a quartz tube reactor and pyrolyzed under an Ar atmosphere at different temperatures (400, 450, 500, 550, and 600 °C) for 1 h at ambient pressure. Thus, molybdenum-based nitrogen carriers were obtained. All NCs were passivated with dilute O_2 (1% O_2 with Ar) for 3 h at room temperature before removing for characteristics.

2.2. Performance evaluation of CLAS with molybdenum-based NCs

All experiments were conducted in an atmospheric fixed-bed reactor (Fig. S1).

In the nitrogen release (ammonia synthesis) step, an H_2 stream (120 NTP ml min^{-1}) was directly introduced to react with the molybdenum-based NCs at their corresponding pyrolysis temperature for 1 h. Then, the vent gas from the reactor was flowed into H_2SO_4 solution (1.0 mmol L^{-1}, 200 ml at 25 °C), and the ammonia production rate was obtained by measuring the decrease in the conductivity of the solution with time [29,30], which can be calculated based on Eq. (1):

$$k = \frac{a \times (\sigma^{*}\text{-}\sigma)}{t_H \times m \times X_T} \quad (1)$$

where k is the rate of ammonia production (μmol g^{-1} h^{-1}); t_H is the hydrogenation time (h); a value of 1.3 can be obtained through the standardization of the change in ionic conductivity with ammonia (details can be found in the Supplementary method); σ^* is the initial conductivity of the solution; while σ is the final conductivity of the solution; m is the mass of the Mo-HMT precursor before pyrolysis; and X_T is the conversion ratio of Mo-HMT to nitride (according to the thermogravimetric (TG) result). All data were collected at a time interval of 3 min

The nitrogen fixation of NC was tested at 600 °C under a N_2 (or N_2 + H_2) atmosphere, in which the flow rate of the gases was 280 NTP ml min^{-1}. The stability of the NC in CLAS was measured by alternately switching the H_2 and N_2/H_2 streams at 600 °C for 1 h. After cooling to room temperature, samples at each step were passivated with dilute O_2 (1% O_2 with Ar) for 3 h, due to air-sensitive of NCs [22]. To avoid the oxidation of the NC, gases with high purity (99.999%) were used, and the reactor was flushed with pure Ar to avoid air and moisture contamination before the performance test.

2.3. Characterization

The weight loss of the Mo-HMT precursor during pyrolysis was analyzed using a TG unit (Mettler Toledo, DSC^{3+}). Typically, 5 mg of precursor was heated under N_2 atmosphere (100 ml min^{-1}) at a heating rate of 10 °C min^{-1} from room temperature to a specified temperature and then maintained at this temperature for 3 h.

The crystalline phases of the samples were measured on a MinFlex600 diffractometer, using Cu K α radiation (λ = 0.15468 nm) as the X-ray source operated at 30 kV and 30 mA. The scan range was performed between 5° and 85° at a scanning rate of 8° min^{-1}.

The surface chemical states of Mo and N in the NCs were determined by X-ray photoelectron spectroscopy (XPS) using a Thermo Scientific K-Alpha+ instrument equipped with an Al Kα anode (hν = 1486.6 eV). All binding energies were referenced to the C 1s peak at 284.8 eV.

The surface morphological characteristics were observed using scanning electron microscopy (SEM, Hitachi SU8100) and transmission electron microscopy (TEM, JEM2100).

The reducibility of the NCs was evaluated by H_2-temperature-programmed reduction (H_2-TPR) on a PCA-1200 equipped with an MS detector under H_2 flow (30 ml min^{-1}) from room temperature to preset temperatures at a slope rate of 5 °C min^{-1}, and the signal of NH_3 (m/z = 17) was monitored.

The Brunauer–Emmett–Teller (BET) surface area of the NCs was determined by nitrogen adsorption at − 196 °C using a Micromeritics ASAP2460 instrument. Before measurement, all samples were vacuum degassed at 200 °C for 3 h to ensure the complete removal of moisture

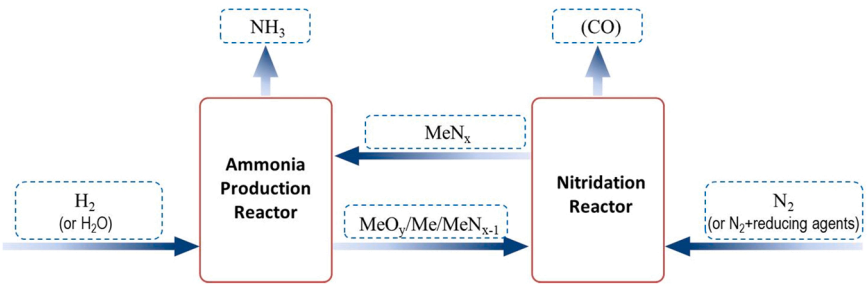

Fig. 1. Schematic diagram of chemical looping ammonia synthesis (CLAS).

and impurities.

The N and H contents of the NCs were determined using a CHNOS elemental analyzer (Vario EL Cube, Elementar Analysensysteme GmbH).

All periodic density functional theory (DFT) calculations in this study were implemented using the Vienna ab initio simulation package (VASP). The electron exchange-correlation was treated using the generalized gradient approximation based on the Perdew, Burke, and Ernzerhof (PBE) functional. The core electrons were described by the projected augmented wave (PAW), and the energy cut-off was selected using a plane wave set to 450 eV. The partial occupancies of the Kohn–Sham orbitals were smeared according to the Methfessel-Paxton smearing method with a width of 0.2 eV. The convergence criterion of geometric optimization for force was smaller than 0.02 eV $Å^{-1}$. Relaxation was terminated when the energy change was less than 10^{-5} eV. A vacuum spacing of 15 Å above the top layer of the plane in the perpendicular direction was imposed to avoid any interaction between the periodic images.

3. Results and discussion

3.1. Characteristics of the NCs prepared under mild conditions

The weight loss of the Mo-HMT precursors during pyrolysis was analyzed using a TG analyzer (Fig. 2). Fig. 2a shows that almost all the curves overlapped before 400 °C, and the final mass of each sample remained almost unchanged at the final synthesis temperature, indicating Mo-based NCs were stable at their corresponding pyrolysis temperatures. Moreover, the final weight loss of the Mo-based NCs increased with increasing pyrolysis temperature (Fig. 2b). The difference between the weight losses could be ascribed to the different contents of nitride-hydride species that evolved during pyrolysis because the N and H amounts of the Mo-based NCs decreased at higher final synthesis temperatures (Table 1). Three obvious troughs were observed in the DTG curve below 280 °C (Fig. 2c). The first likely arose from the loss of water and the latter two from dehydration and ammonia production [31]. At higher temperatures, the slightly flat curves can be attributed to the evolution of CO, according to our previous study [32].

The XRD patterns of the Mo-based NCs obtained at different temperatures are shown in Fig. 3a. NCs tended to be amorphous at lower temperatures (400 and 450 °C), and the peak intensity of the NCs became stronger as the synthesis temperature increased. In particular, the diffraction peaks at approximately 37.4°, 43.5°, 63.1°, 75.7°, and 79.7° correspond to the (111), (200), (220), (311), and (222) facets of γ-Mo_2N (PDF #25-1366), respectively, indicating the successful synthesis of Mo-based NCs by the facile pyrolysis method. In addition, no peaks related to the molybdenum oxide phase were observed for the Mo-based NCs.

Mo-based NC obtained at 600 °C was chosen for subsequent studies. The surface chemical oxidation states of the Mo-based NC were analyzed using XPS in the full spectrum (Fig. S2a). Distinct peaks positioned at approximately 230.8, 284.2, 400.0, 411.2, and 530.1 eV were attributed to Mo 3d, C 1s, N 1s, Mo 3p, and O 1s, respectively. The presence of the O 1s peak indicates that the oxidation of the sample occurred after passivation. The presence of Mo_2N was also verified by the XPS spectrum of Mo 3d (Fig. 3b) and N 1s (Fig. S2b). The deconvolution of the Mo 3d spectra yielded Mo 3d doublets, which correspond to $Mo^{\delta+}$ (where $0 < \delta < 4$) [33], Mo^{4+}, and Mo^{6+}, respectively. The binding energies (BEs) of 228.4 and 231.5 eV can be assigned to $Mo^{\delta+}$ $3d_{5/2}$ and $Mo^{\delta+}$ $3d_{3/2}$ of nitride, respectively. While the other Mo 3d peak at 229.9 and 232.7 eV can be associated with Mo^{4+} species as in MoO_2, the peaks at 232.5 and 235.2 eV can be attributed to MoO_3 with a valence state of Mo^{6+}. The presence of Mo^{4+} and Mo^{6+} can be ascribed to the surface oxidation of Mo nitride during passivation. For the XPS spectrum of N 1s (Fig. S2b), the peaks at 394.5 and 397.0 eV can be assigned to the Mo 3p and the typical binding indicator of Mo—N bond [33]. The other two peaks at 398.6 and 400.0 eV correspond to pyridinic-N and pyrrolic-N, respectively [34].

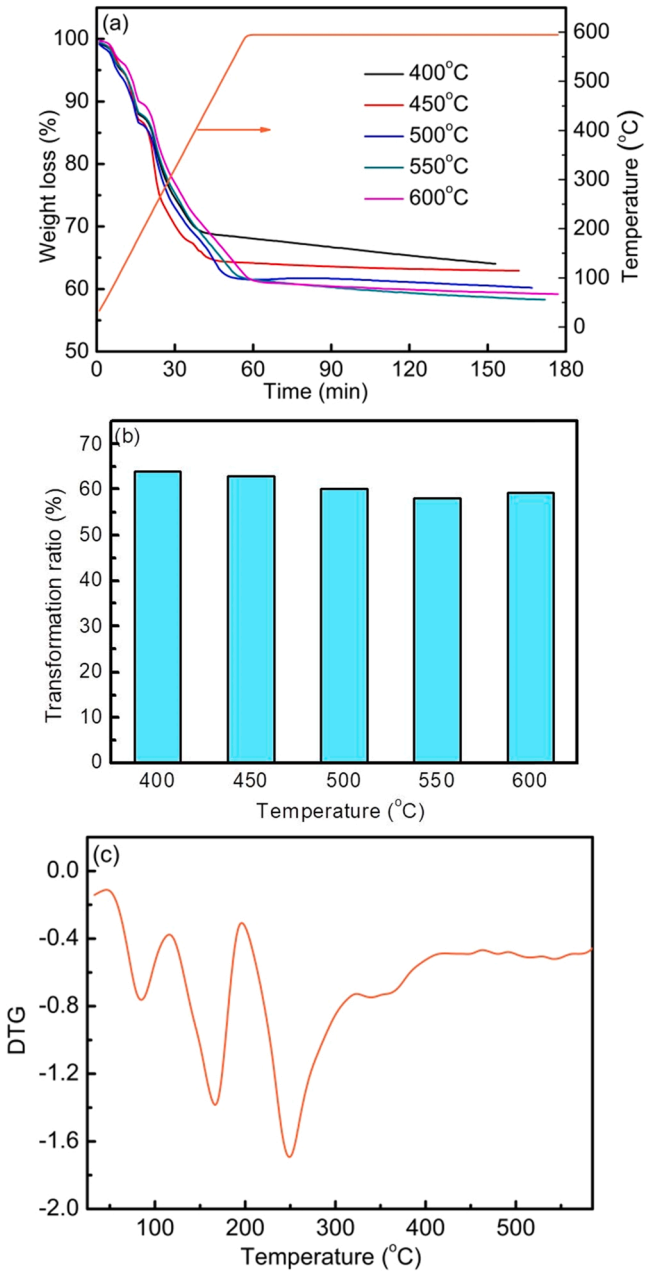

Fig. 2. TGA result of Mo-HMT precursor. (a) Weight loss. (b) Transformation ratio of Mo-based NCs at different temperatures. (c) DTG curve of the Mo-based NCs pyrolyzed at 600 °C.

Table 1
N and H contents of Mo-based NCs obtained at different temperatures.

Pyrolysis temperature (°C)	N (wt%)	H (wt%)
400	5.349	0.718
450	5.619	0.687
500	5.422	0.555
550	5.244	0.529
600	4.678	0.451

Clear lattice fringes with a spacing of 0.241 nm were observed (Fig. 3c), which correspond to the (111) planes of γ-Mo_2N, in line with our previous finding [28]. Highly magnified SEM images clearly show rod-like shapes with flat surfaces and a length of approximately 30 μm

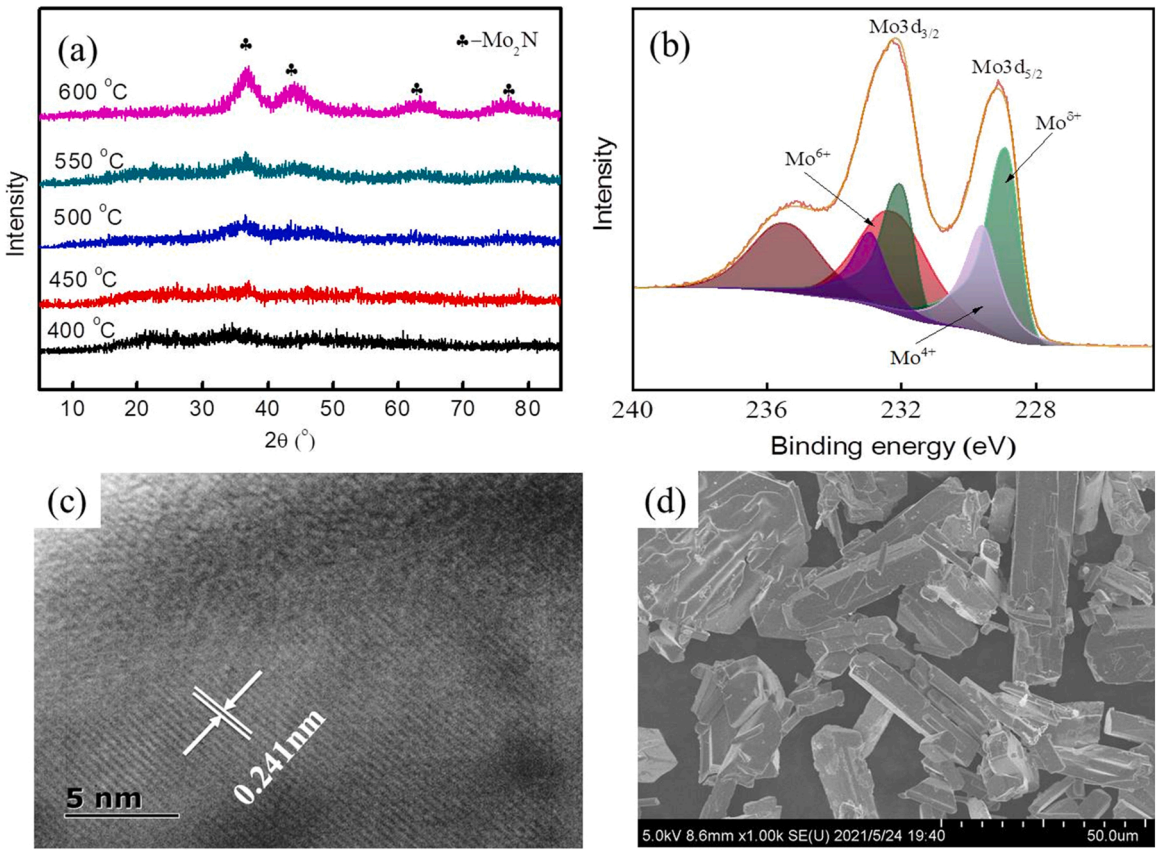

Fig. 3. Mo-based NCs obtained by the pyrolysis of Mo-HMT precursors: (a) XRD patterns of samples pyrolyzed at different temperatures and (b) High-resolution XPS spectra of Mo 3d. (c) TEM and (d) SEM images of Mo-based NC prepared at 600 °C.

(Fig. 3d), consistent with the results of other studies [32]. Comparisons of the SEM images of Mo-based NCs acquired at different pyrolysis temperatures are shown in Fig. S3. No obvious differences in the morphology of the NCs were observed, and the particle size distribution was between 24 and 50 μm.

3.2. Ammonia synthesis performance of molybdenum based NCs

NH_3 formation during H_2 introduction was confirmed using Nessler's reagent method. As shown in Fig. S4, no color change was observed in the blank experiment, whereas the color of the solution changed from colorless to brown upon venting gas, indicating the successful generation of NH_3 on H_2 introduction. To further verify ammonia generation, the mass signal of the pyrolyzed Mo-based NC at 450 °C was tested using H_2-TPR-MS. As shown in Fig. S5, the ammonia signal was monitored for Mo-based NC at temperatures above 300 °C.

The NH_3 release characteristics of the NCs were quantitatively analyzed at preset temperatures. Fig. 4a shows that the ammonia production rates of the NCs were faster at the initial stage and then decreased with prolonged reaction time. Notably, the NH_3 production curve of NC obtained at 450 °C outperformed that of the other NCs. The average NH_3 production rate of the Mo-based NCs was calculated for the first 60 min of hydrogenation. Fig. 4b shows that the NH_3 production rates of Mo-based NCs peaked at 450 °C at a rate of 4576 μmol g^{-1} h^{-1}, and the average NH_3 production rate decreased with further increase in pyrolysis temperature (Fig. 4b), which could be ascribed to the different

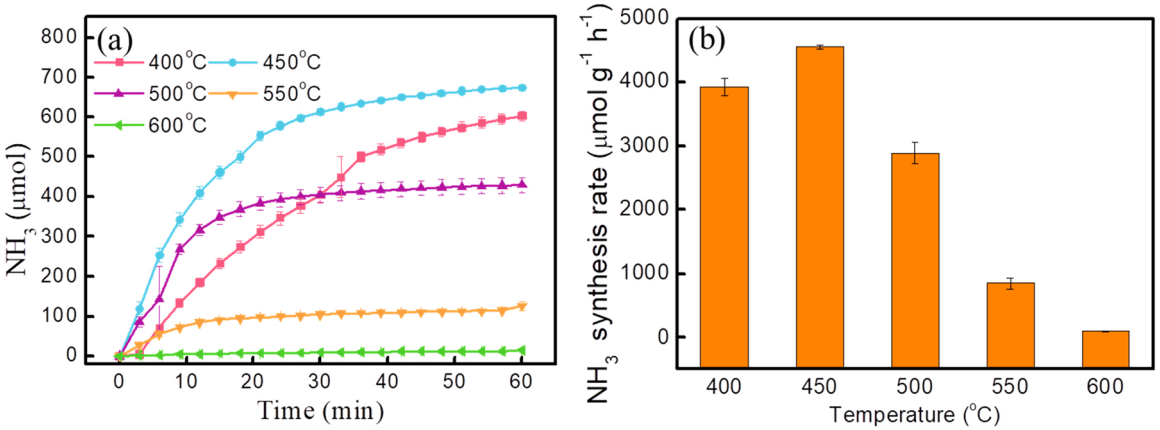

Fig. 4. (a) Ammonia yields and (b) average ammonia production rates of Mo-based NCs with H_2 at different temperatures (WHSV = 60,000 ml g^{-1} h^{-1}).

reactivities of lattice nitrogen on the NCs obtained at different synthesis temperatures.

The reactivity of lattice nitrogen is also a decisive factor in the selection of appropriate NC candidates. The lattice nitrogen of transition metal nitrides was found to be either reactive toward H_2 to generate NH_3 or directly released as N_2 [35]. Nitrogen occupies the interstitial spaces between the parent Mo atoms. At the N release step, a substantial amount of lattice nitrogen was removed from the nitride structure and nitrogen vacancies remained. Therefore, the mass balance of N during the N release stage was calculated, as shown in Table 2 and Fig. 5. The NH_3 generation rate decreased with increasing temperature, while the N_2 production rate was more favorable at higher temperatures. For example, 52% of lattice nitrogen in the NC obtained at 450 °C was liberated, among which 39% of the lattice nitrogen was transformed into NH_3 and 13% was lost as N_2.

The Mo-based NC after hydrogenation at 600 °C were analyzed in detail. Fig. 6a compares the XRD patterns of NC before and after hydrogenation. Compared to the pyrolysis sample, three new peaks at 40.5°, 58.6°, and 73.7° were observed for the hydrogenated one, corresponding to (110), (200), and (211) of Mo (PDF #42-1120), respectively. The phase transformation from Mo_2N to Mo suggests the release of lattice nitrogen from NC, which is consistent with ammonia generation during hydrogenation (Fig. 4).

The surface chemical compositions and valence states of the elements after hydrogenation at 600 °C were investigated using XPS (Figs. 6b and S6). Fig. 6b plots the narrow scans of Mo 3d that can be deconvoluted into six peaks. Peaks at 227.6 ($3d_{5/2}$) and 230.8 eV can be assigned to Mo [36], a reduction product of NC, those at 228.9 and 231.8 eV could be assigned to $Mo^{\delta+}$ species, whereas the higher binding energy (BE) Mo $3d_{5/2}$ peak at 229.9 eV and its shakeup satellites were due to MoO_2 with a chemical state of Mo^{4+} [33]. For the XPS spectrum of N 1 s XPS spectrum (Fig. S6b), the peak at 396.6 eV can be attributed to the typical binding indicator of the Mo-N bond. Compared with Fig. S2b, the BE shift to lower values provides evidence that Mo_2N receives electrons to generate Mo [37].

Lattice fringes with a spacing of 0.220 nm were observed in the TEM image of the post-hydrogenated sample (Fig. 5c), which correspond to the lattice distance of Mo (110) [38]. Comparing the SEM images of the pyrolysis sample (Fig. 3d) shows that the hydrogenated sample had an uneven and cracked surface (Fig. 6d), which is in good agreement with the increase in surface area (Table 3). A similar phenomenon was observed for the other samples after hydrogenation at different temperatures (Fig. S7). The cracked surfaces of NCs could be due to the lattice stress and defects of NC in different forms during cyclic CLAS operation [39–42].

The NH_3 production performance of Mo-based NC via CLAS and the thermocatalytic process were compared, as shown in Fig. 7. It is worth mentioning that the NH_3 production rates of CLAS were three times higher than those of the thermo-catalytic process by co-feeding mixed N_2-$3H_2$ for 60 min. In addition, Table S1 compares the ammonia production rates of Mo-based NC with those of some known transition/alkaline earth metal nitrides developed at atmospheric pressure and low temperatures [43,44]. The Mo-based NC performed markedly well under milder conditions, and its NH_3 production rate was one or two orders of magnitude higher than those of other transition/alkaline earth metal nitrides.

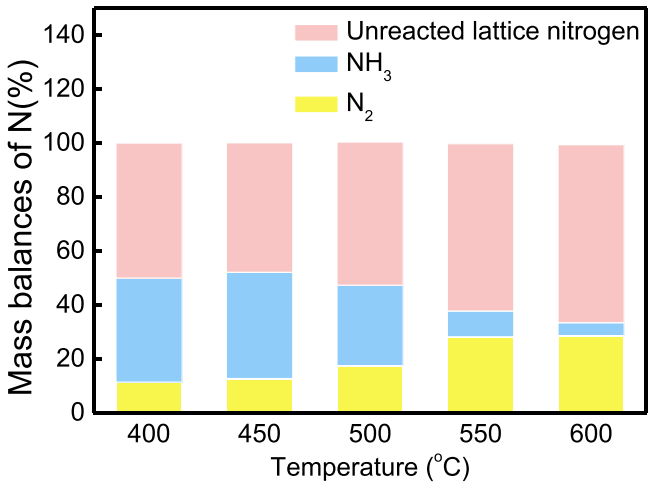

Fig. 5. Mass balances of N during the N release step of NCs obtained at different temperatures.

3.3. Nitrogen fixation performance of molybdenum based NCs

The efficient regenerability of Mo-based NCs is key to the practical feasibility and competitiveness of CLAS. However, the regeneration of transition metals with N_2 at ambient pressure is difficult due to their low kinetics [26,45]. We regenerated Mo using pure nitrogen; no significant Mo_2N phase was formed despite the long reaction time of 15 h (Fig. S8), demonstrating the slow nitrogen-fixation kinetics of Mo. The inclusion of H_2 in the N_2 feed is helpful for the enhancement of nitrogen-fixing kinetics for N-poor nitride [46–48]. Hence, H_2 was introduced to regenerate Mo-based NCs in this study.

During the N-fixation step, the nitrogen vacancies were refilled via N_2 reduction. Fig. 8a compares the XRD patterns of the nitridized NCs. With an increase in the H_2 proportion, the Mo peaks gradually disappeared, while the intensities of Mo_2N increased, indicating the successful regeneration of Mo-based NCs with the aid of H_2 introduction in the N_2 feed. Small peaks related to MoO_2 (PDF #32-0671) were observed for the nitridized NCs, which could be attributed to the slight oxidation of NC during the N fixation process. Nitrogen fixation was further verified by elemental analysis of NCs. As shown in Table 3, the N content of Mo-based NC decreased from 4.678 to 3.879 wt% after hydrogenation, while it was replenished to 5.451 wt% after regeneration under an atmosphere of $H_2/N_2 = 3:1$. NCs prepared by facile pyrolysis contain some C and O impurities [31], and the content of these impurities decreased with increasing pyrolysis temperature. However, the C/O cannot be replenished during the N-fixation step, which leads to a higher N content in the spent NC than in the fresh one (Table 3). Meanwhile, the Mo peak shift of 0.3 eV toward higher binding energy (Fig. 8b) and the typical binding indicator of Mo—N bond in N 1s spectrum shifted to higher BE (Fig. S9) were observed after nitrogen

Table 2
N mass balances during N release step with NCs obtained at different temperatures.

Hydrogenation temperature/°C	Nitrogen content/wt%		Mass conversion ratio	Total N content/ μmol/g	NH_3 produced/ μmol/g	% lattice N lost converted to NH_3	% lattice N lost converted to N_2
	Pre-reaction	Post-reaction					
400	5.349	3.289	0.8117	3820.71	1475.75	39	11
450	5.619	3.146	0.8535	4013.57	1580.73	39	13
500	5.422	3.349	0.8510	3872.86	1156.72	30	18
550	5.244	3.915	0.8329	3745.71	355.49	9	28
600	4.678	3.879	0.8019	3341.43	160.64	5	29

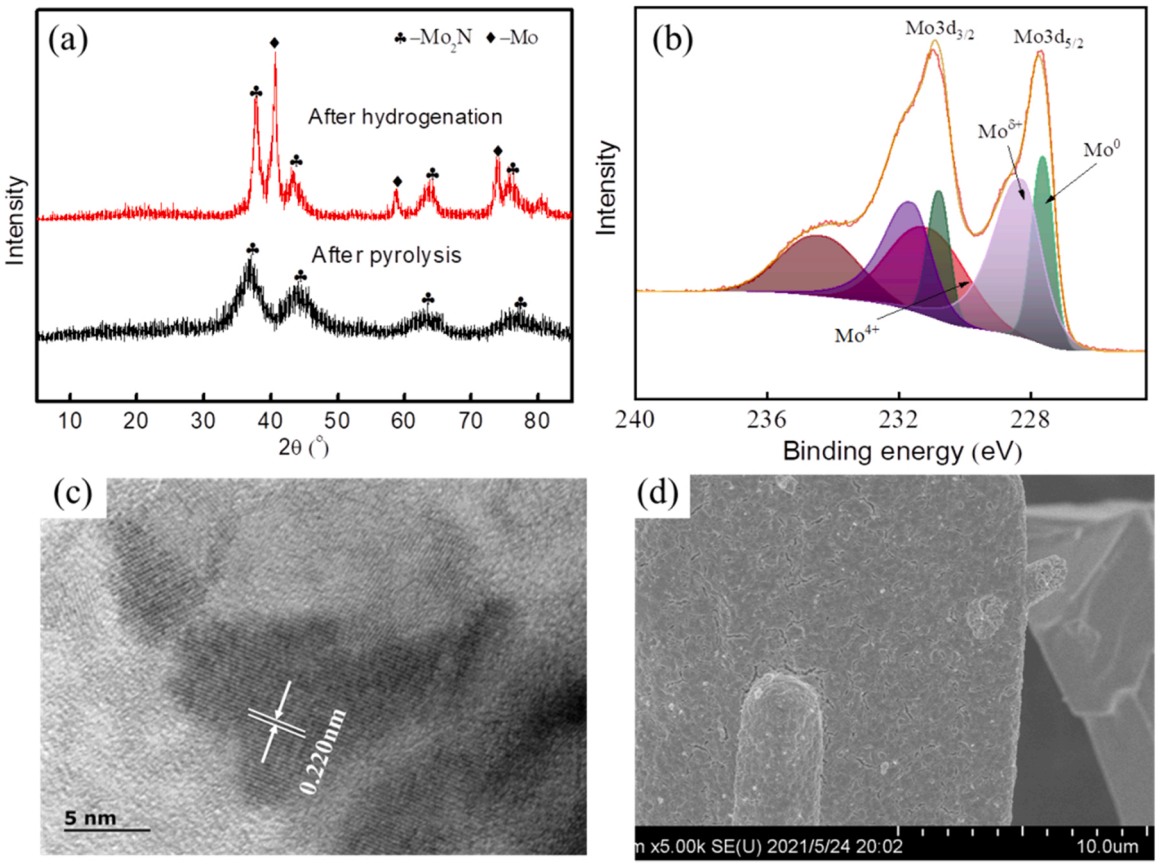

Fig. 6. Post-hydrogenated samples at 600 °C: (a) XRD patterns of Mo-based NCs after pyrolysis (black line) and after hydrogenation (red line); (b) High-resolution XPS spectra of Mo 3d for the hydrogenation sample; images of (c) TEM and (d) SEM.

Table 3
Nitrogen content and specific surface area of samples[a].

Sample	N (wt%)	BET ($m^2\ g^{-1}$)
After pyrolysis	4.678	0.2365
After hydrogenation	3.879	1.2847
After regeneration[b]	5.451	1.5214

[a] Samples were all obtained at 600 °C.
[b] Regeneration of Mo-based NC was conducted under an H_2/N_2 atmosphere with a ratio of 3/1.

fixation, indicating electron transfer from Mo to generate Mo_2N. The lattice fringes with a spacing of 0.241 nm in the TEM pattern (Fig. 8c) corresponded to the (111) planes of Mo_2N. Fig. 8d shows scanning electron microscopy (SEM) images of the prepared regeneration sample; no significant changes were observed in the particle size in length compared with that of the NCs after pyrolysis and hydrogenation (Figs. 2d and 4d).

DFT calculations were conducted to understand the effect of H_2 introduction on nitrogen fixation with Mo-based NC, as shown in Fig. 9. Detailed information on the DFT model is presented in Table S2. In addition, the free energies for Mo + N_2 to Mo + 2N with and without H_2 at 600 °C were compared (Fig. 9). N_2 was adsorbed onto the pure Mo (110) surface in the initial reaction structure. On N_2 dissociation, the

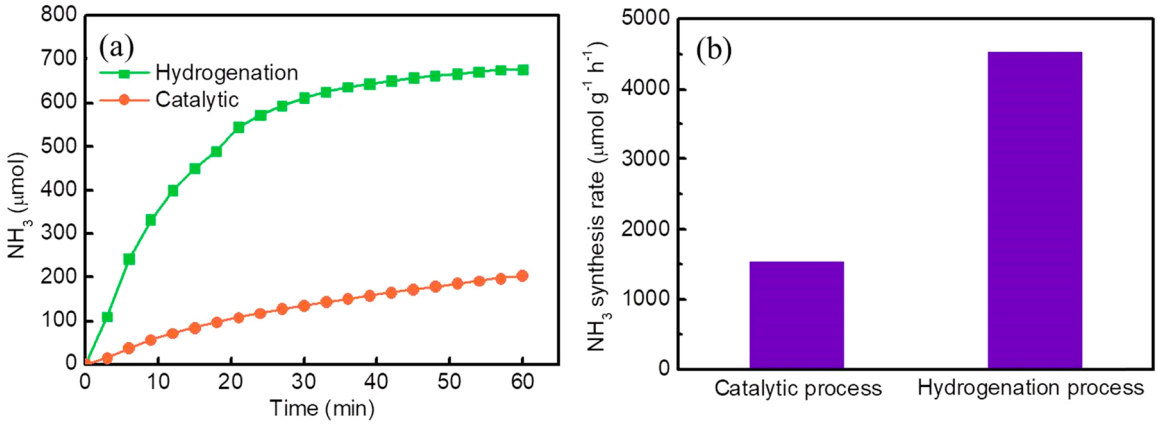

Fig. 7. Comparison of NH_3 production rates in hydrogenation of chemical looping and thermo-catalytic processes at 450 °C and 1 bar (WHSV = 60,000 ml $g^{-1}\ h^{-1}$).

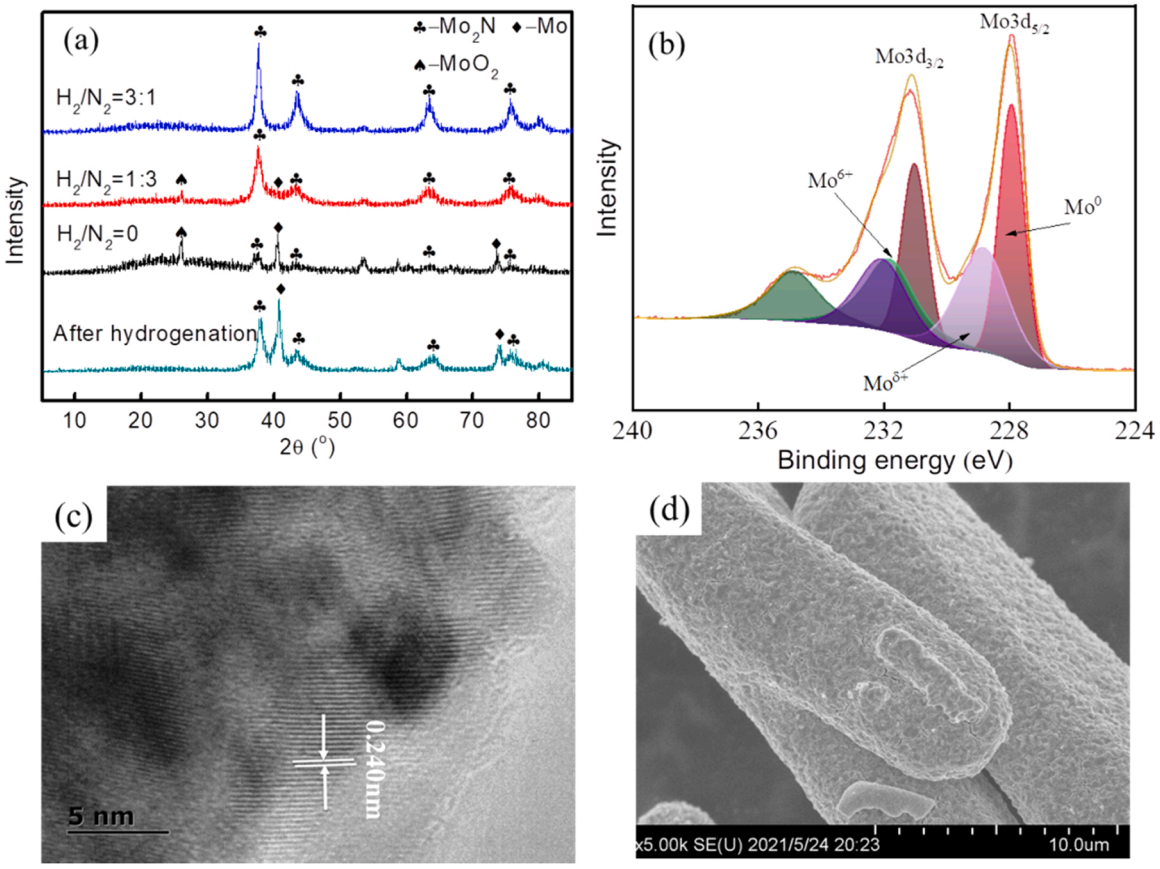

Fig. 8. Post-nitridized samples: (a) XRD patterns of nitridized samples under different H_2/N_2 atmospheres at 600 °C for 60 min, (b) High-resolution XPS spectra of Mo 3d, (c) TEM and (d) SEM images of the regenerated sample with H_2/N_2 = 3:1 at 600 °C.

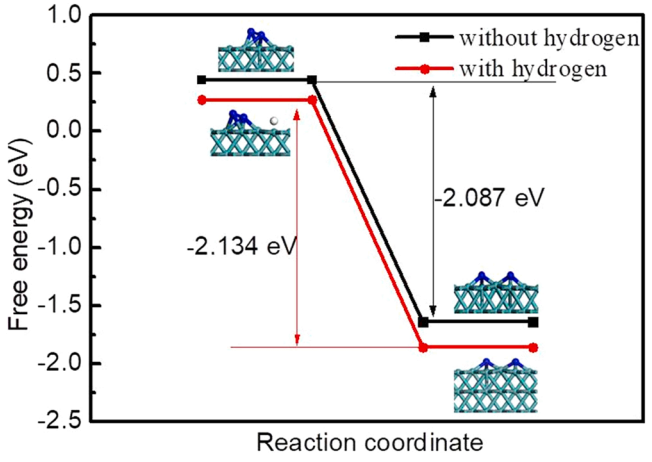

Fig. 9. Density functional theory (DFT) calculations: free energies of regeneration process for Mo + N_2 to Mo + 2N at 600 °C.

free energy change was − 2.087 eV. When there were H atoms, the free energy change of the above process was − 2.134 eV. The ΔG value with hydrogen (− 2.134 eV) was lower than that without hydrogen (−2.087 eV), suggesting N_2 was easily dissociated, and the subsequent reaction between N_2 and Mo occurred more easily in the presence of H_2.

3.4. Cyclic performance of molybdenum based NCs

The stability of Mo-based NC was evaluated at 600 °C and atmospheric pressure. Fig. 10 shows that the ammonia production rate slowly decreased compared with that in the first cycle and the ammonia production rate remained at approximately 100 μmol g^{-1} h^{-1}. The cycled NC sample was further characterized using X-ray diffraction, XPS, TEM, and SEM. The reflections related to Mo and Mo_2N are shown in Fig. 11a. Moreover, the presence of MoO_2 indicated that the slight deactivation of NC could be caused by a trace amount of oxygen during the stability test. The coexistence of $Mo^{\delta+}$ and Mo in the continuous denitridation and nitridation cycles of the sample was evidenced by a shoulder observed in the main peak at 227.5 eV, which was assigned to Mo, as shown in Fig. 11b. The higher binding energy Mo $3d_{5/2}$ peak at 228.5 eV can be

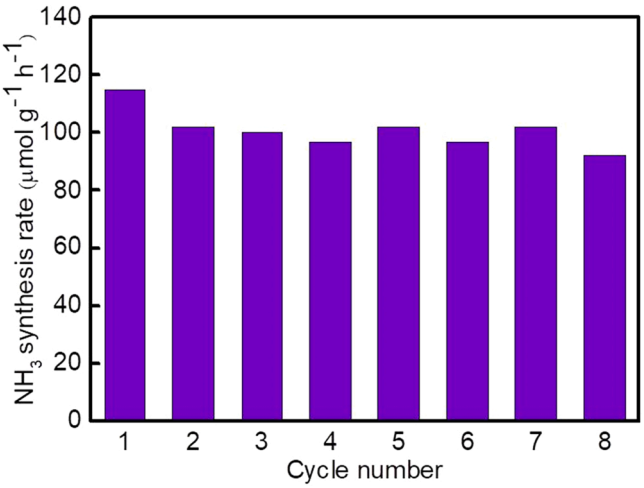

Fig. 10. Cyclic tests of Mo-based NC at 600 °C and 1 bar.

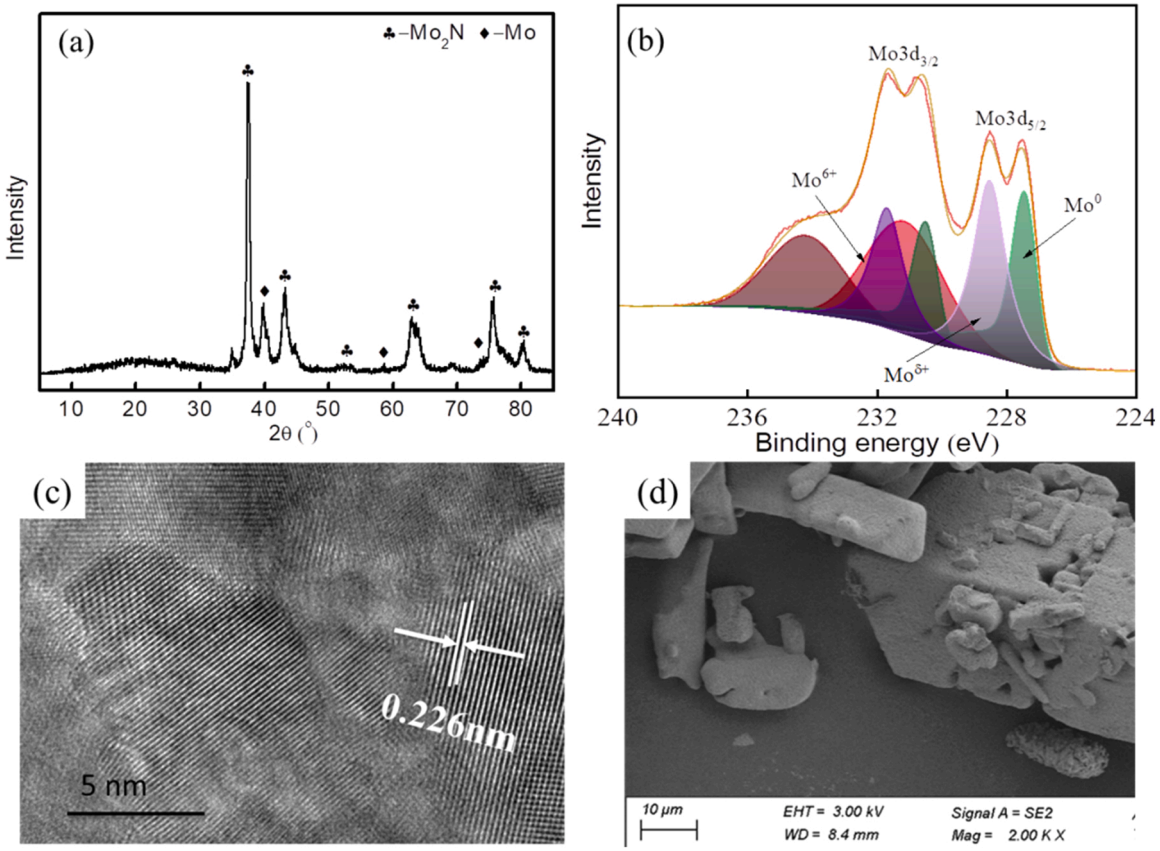

Fig. 11. (a) XRD patterns, (b) High-resolution XPS spectra of Mo 3d, and (c) TEM and (d) SEM images for used Mo-based NC after cyclic test at 600 °C and 1 bar.

attributed to $Mo^{\delta+}$. The other peaks were associated with molybdenum oxide (MoO_3). According to the HRTEM image (Fig. 11c), the lattice fringes with a spacing of 0.226 nm can be ascribed to the distance between the lattice planes of Mo (110). From morphological observations (Fig. 11d), no significant difference was detected in particle size compared with the sample after the first cycle. After the stability test, no significant changes in the phase, surface chemical states, and morphology were observed, indicating that Mo-based NCs possess favorable stability.

4. Conclusions

A looped ammonia synthesis process mediated by the Mo_2N/Mo pair was reported and presented in this work. Mo-based NCs were facilely synthesized at different temperatures and the performance of N-discharge, N-charge, and NC stability were analyzed in detail. The results indicate that Mo-based NCs have excellent ammonia production rate, high N-fixation efficiency, and good stability. In the N-release process, the chemical looping process produces NH_3 with an average rate above 4576 μmol g^{-1} h^{-1}, and it is important to note that the chemical looping process increased the NH_3 production rate by a factor of 3 over that through the thermo-catalytic process at 450 °C and atmospheric pressure. In the N-fixation process, the presence of H_2 strongly accelerated the nitridation rates between Mo and N_2. Finally, NC produced ammonia without a significant rate decrease in the cyclic CLAS test.

CRediT authorship contribution statement

Song Yang, Tan Zhang: Conceptualization, Investigation, Validation, Formal analysis, Writing – original draft, Writing – review & editing. **Yanyan Yang, Bixi Wang, Jin Li, Zhouting Gong, Zhengyue Yao, Wenguang Du:** Investigation, Validation. **Shoujun Liu, Zhongliang Yu**: Conceptualization, Resources, Visualization, Supervision, Writing – review & editing.

Declaration of Competing Interest

The authors declare that they have no known competing financial interests or personal relationships that could have appeared to influence the work reported in this paper.

Acknowledgements

This work is supported by National Natural Science Foundation of China (Nos. 22169017 and 51976226) and the Science and Technology Project of Jiangxi Education Department (GJJ201709).

Appendix A. Supporting information

Supplementary data associated with this article can be found in the online version at doi:10.1016/j.apcatb.2022.121404.

References

[1] G. Soloveichik, Electrochemical synthesis of ammonia as a potential alternative to the Haber-Bosch process, Nat. Catal. 2 (2019) 377–380, https://doi.org/10.1038/s41929-019-0280-0.
[2] B.H.R. Suryanto, H.L. Du, D.B. Wang, J. Chen, A.N. Simonov, D.R. MacFarlane, Challenges and prospects in the catalysis of electroreduction of nitrogen to ammonia, Nat. Catal. 2 (2019) 290–296, https://doi.org/10.1038/s41929-019-0252-4.
[3] Z. Li, Z. Ma, J. Liang, Y. Ren, T. Li, S. Xu, Q. Liu, N. Li, B. Tang, Y. Liu, S. Gao, A. A. Alshehri, D. Ma, Y. Luo, Q. Wu, X. Sun, MnO_2 nanoarray with oxygen vacancies: an efficient catalyst for NO electroreduction to NH_3 at ambient conditions, Mater. Today Phys. 22 (2022), https://doi.org/10.1016/j.mtphys.2021.100586.

[4] S. Li, Y. Wang, J. Liang, T. Xu, D. Ma, Q. Liu, T. Li, S. Xu, G. Chen, A.M. Asiri, Y. Luo, Q. Wu, X. Sun, TiB_2 thin film enabled efficient NH_3 electrosynthesis at ambient conditions, Mater. Today Phys. 18 (2021), https://doi.org/10.1016/j.mtphys.2021.100396.

[5] L. Zhang, J. Liang, Y. Wang, T. Mou, Y. Lin, L. Yue, T. Li, Q. Liu, Y. Luo, N. Li, B. Tang, Y. Liu, S. Gao, A.A. Alshehri, X. Guo, D. Ma, X. Sun, High-performance electrochemical NO reduction into NH_3 by MoS_2 nanosheet, Angew. Chem. Int. Ed. Engl. 60 (2021) 25263–25268, https://doi.org/10.1002/anie.202110879.

[6] S. Li, Y. Wu, Q. Liu, B. Li, T. Li, H. Zhao, A.A. Alshehri, K.A. Alzahrani, Y. Luo, L. Li, X. Sun, CuS concave polyhedral superstructures enabled efficient N_2 electroreduction to NH_3 at ambient conditions, Inorg. Chem. Front. 8 (2021) 3105–3110, https://doi.org/10.1039/d1qi00306b.

[7] G. Wen, J. Liang, Q. Liu, T. Li, X. An, F. Zhang, A.A. Alshehri, K.A. Alzahrani, Y. Luo, Q. Kong, X. Sun, Ambient ammonia production via electrocatalytic nitrite reduction catalyzed by a CoP nanoarray, Nano Res. 15 (2021) 972–977, https://doi.org/10.1007/s12274-021-3583-9.

[8] T. Xu, J. Liang, Y. Wang, S. Li, Z. Du, T. Li, Q. Liu, Y. Luo, F. Zhang, X. Shi, B. Tang, Q. Kong, A.M. Asiri, C. Yang, D. Ma, X. Sun, Enhancing electrocatalytic N_2-to-NH_3 fixation by suppressing hydrogen evolution with alkylthiols modified Fe_3P nanoarrays, Nano Res. 15 (2021) 1039–1046, https://doi.org/10.1007/s12274-021-3592-8.

[9] Q. Wang, J. Guo, P. Chen, Recent progress towards mild-condition ammonia synthesis, J. Energy Chem. 36 (2019) 25–36, https://doi.org/10.1016/j.jechem.2019.01.027.

[10] J.L. Hua, K. Wang, Q. Wang, R.J. Peng, Feasibility of Fe-based nitrogen carrier for chemical looping ammonia synthesis: thermodynamics, J. Therm. Anal. Calorim. 146 (2021) 673–680, https://doi.org/10.1007/s10973-020-10029-x.

[11] M.E. Galvez, A. Frei, M. Halmann, A. Steinfeld, Ammonia production via a two-step Al_2O_3/AlN thermochemical cycle. 2. Kinetic analysis, Ind. Eng. Chem. Res. 46 (2007) 2047–2053, https://doi.org/10.1021/ie061551m.

[12] Y. Wu, Y. Gao, Q. Zhang, T. Cai, X. Chen, D. Liu, M. Fan, Promising zirconia-mixed Al-based nitrogen carriers for chemical looping of NH_3: reduced NH_3 decomposition and improved NH_3 yield, Fuel 264 (2020), https://doi.org/10.1016/j.fuel.2019.116821.

[13] Y. Gao, Y. Wu, Q. Zhang, X. Chen, G. Jiang, D. Liu, N-desorption or NH_3 generation of TiO_2-loaded Al-based nitrogen carrier during chemical looping ammonia generation technology, Int. J. Hydrog. Energy 43 (2018) 16589–16597, https://doi.org/10.1016/j.ijhydene.2018.07.042.

[14] D.F. Swearer, N.R. Knowles, H.O. Everitt, N.J. Halas, Light-driven chemical looping for ammonia synthesis, ACS Energy Lett. 4 (2019) 1505–1512, https://doi.org/10.1021/acsenergylett.9b00860.

[15] R. Michalsky, P.H. Pfromm, Chromium as reactant for solar thermochemical synthesis of ammonia from steam, nitrogen, and biomass at atmospheric pressure, Sol. Energy 85 (2011) 2642–2654, https://doi.org/10.1016/j.solener.2011.08.005.

[16] M.G. Heidlage, E.A. Kezar, K.C. Snow, P.H. Pfromrn, Thermochemical synthesis of ammonia and syngas from natural gas at atmospheric pressure, Ind. Eng. Chem. Res. 56 (2017) 14014–14024, https://doi.org/10.1021/acs.iecr.7b03173.

[17] W. Gao, P. Wang, J. Guo, F. Chang, T. He, Q. Wang, G. Wu, P. Chen, Barium hydride-mediated nitrogen transfer and hydrogenation for ammonia synthesis: a case study of cobalt, ACS Catal. 7 (2017) 3654–3661, https://doi.org/10.1021/acscatal.7b00284.

[18] W. Gao, J. Guo, P. Wang, Q. Wang, F. Chang, Q. Pei, W. Zhang, L. Liu, P. Chen, Production of ammonia via a chemical looping process based on metal imides as nitrogen carriers, Nat. Energy 3 (2018) 1067–1075, https://doi.org/10.1038/s41560-018-0268-z.

[19] S. Feng, W. Gao, Q. Wang, Y. Guan, H. Yan, H. Wu, H. Cao, J. Guo, P. Chen, A multi-functional composite nitrogen carrier for ammonia production via a chemical looping route, J. Mater. Chem. A 9 (2021) 1039–1047, https://doi.org/10.1039/d0ta10519h.

[20] W.M. Aframehr, C. Huang, P.H. Pfromm, Chemical looping of manganese to synthesize ammonia at atmospheric pressure: sodium as promoter, Chem. Eng. Technol. 43 (2020) 2126–2133, https://doi.org/10.1002/ceat.202000154.

[21] R. Michalsky, A.M. Avram, B.A. Peterson, P.H. Pfromm, A.A. Peterson, Chemical looping of metal nitride catalysts: low-pressure ammonia synthesis for energy storage, Chem. Sci. 6 (2015) 3965–3974, https://doi.org/10.1039/c5sc00789e.

[22] R. Kojima, K. Aika, Molybdenum nitride and carbide catalysts for ammonia synthesis, Appl. Catal. A-Gen. 219 (2001) 141–147, https://doi.org/10.1016/S0926-860x(01)00676-7.

[23] N. Bion, F. Can, J. Cook, J.S.J. Hargreaves, A.L. Hector, W. Levason, A. R. McFarlane, M. Richard, K. Sardar, The role of preparation route upon the ambient pressure ammonia synthesis activity of Ni_2Mo_3N, Appl. Catal. A: Gen. 504 (2015) 44–50, https://doi.org/10.1016/j.apcata.2014.10.030.

[24] X. Ren, G. Cui, L. Chen, F. Xie, Q. Wei, Z. Tian, X. Sun, Electrochemical N_2 fixation to NH_3 under ambient conditions: Mo_2N nanorod as a highly efficient and selective catalyst, Chem. Commun. 54 (2018) 8474–8477, https://doi.org/10.1039/c8cc03627f.

[25] Y. Abghoui, A.L. Garden, J.G. Howalt, T. Vegge, E. Skúlason, Electroreduction of N_2 to ammonia at ambient conditions on mononitrides of Zr, Nb, Cr, and V: a DFT guide for experiments, ACS Catal. 6 (2015) 635–646, https://doi.org/10.1021/acscatal.5b01918.

[26] R. Michalsky, P.H. Pfromm, A. Steinfeld, Rational design of metal nitride redox materials for solar-driven ammonia synthesis, Interface Focus 5 (2015), 20140084, https://doi.org/10.1098/rsfs.2014.0084.

[27] R. Michalsky, B.J. Parman, V. Amanor-Boadu, P.H. Pfromm, Solar thermochemical production of ammonia from water, air and sunlight: thermodynamic and economic analyses, Energy 42 (2012) 251–260, https://doi.org/10.1016/j.energy.2012.03.062.

[28] Z. Yu, X. An, I. Kurnia, A. Yoshida, Y. Yang, X. Hao, A. Abudula, Y. Fang, G. Guan, Full spectrum decomposition of formic acid over γ-Mo_2N-based catalysts: from dehydration to dehydrogenation, ACS Catal. 10 (2020) 5353–5361, https://doi.org/10.1021/acscatal.0c00752.

[29] D. McKay, D.H. Gregory, J.S. Hargreaves, S.M. Hunter, X. Sun, Towards nitrogen transfer catalysis: reactive lattice nitrogen in cobalt molybdenum nitride, Chem. Commun. (2007) 3051–3053, https://doi.org/10.1039/b707913c.

[30] K. Sato, K. Imamura, Y. Kawano, S. Miyahara, T. Yamamoto, S. Matsumura, K. Nagaoka, A low-crystalline ruthenium nano-layer supported on praseodymium oxide as an active catalyst for ammonia synthesis, Chem. Sci. 8 (2017) 674–679, https://doi.org/10.1039/c6sc02382g.

[31] P. Afanasiev, New single source route to the molybdenum nitride Mo_2N, Inorg. Chem. 41 (2002) 5317–5319, https://doi.org/10.1021/ic025564d.

[32] Z. Yu, A. Yoshida, J. Shi, T. Wang, S. Yang, Q. Ye, X. Hao, A. Abudula, Y. Fang, G. Guan, Formic acid as a Bio-CO carrier: selective dehydration with γ-Mo_2N catalysts at low temperatures, ACS Sustain. Chem. Eng. 8 (2020) 13956–13963, https://doi.org/10.1021/acssuschemeng.0c03269.

[33] Z.B.Z. Wei, P. Grange, B. Delmon, XPS and XRD studies of fresh and sulfided Mo_2N, Appl. Surf. Sci. 135 (1998) 107–114, https://doi.org/10.1016/S0169-4332(98)00267-0.

[34] Y.J. Song, Z.Y. Yuan, One-pot synthesis of Mo_2N/NC catalysts with enhanced electrocatalytic activity for hydrogen evolution reaction, Electrochim. Acta 246 (2017) 536–543, https://doi.org/10.1016/j.electacta.2017.06.086.

[35] R. Michalsky, P.H. Pfromm, An ionicity rationale to design solid phase metal nitride reactants for solar ammonia production, J. Phys. Chem. C 116 (2012) 23243–23251, https://doi.org/10.1021/jp307382r.

[36] L. Assmann, J.C. Bernède, A. Drici, C. Amory, E. Halgand, M. Morsli, Study of the Mo thin films and Mo/CIGS interface properties, Appl. Surf. Sci. 246 (2005) 159–166, https://doi.org/10.1016/j.apsusc.2004.11.020.

[37] D. Nikolova, R. Edrevakardjieva, G. Gouliev, T. Grozeva, P. Tzvetkov, The state of (K)(Ni)Mo/γ-Al_2O_3 catalysts after water–gas shift reaction in the presence of sulfur in the feed: XPS and EPR study, Appl. Catal. A: Gen. 297 (2006) 135–144, https://doi.org/10.1016/j.apcata.2005.08.043.

[38] A. Madan, X. Chu, S.A. Barnett, Growth and characterization of epitaxial Mo/NbN superlattices, Appl. Phys. Lett. 68 (1996) 2198–2200, https://doi.org/10.1063/1.116011.

[39] Z.-l Liu, M. Meng, Y.-l Fu, M. Jiang, T.-d Hu, Y.-n Xie, T. Liu, EXAFS study of γ-Mo_2N and Mo nitrides supported on zeolites, Mater. Lett. 54 (2002) 364–371, https://doi.org/10.1016/s0167-577x(01)00595-x.

[40] M. Giovanni, A. Ambrosi, Z. Sofer, M. Pumera, Impact electrochemistry of individual molybdenum nanoparticles, Electrochem. Commun. 56 (2015) 16–19, https://doi.org/10.1016/j.elecom.2015.04.002.

[41] F. Martin, J. Pacaud, G. Abadias, C. Jaouen, P. Guerin, Strains and stresses in an epitaxial Ni(111)/Mo(110) multilayer grown by direct ion beam sputtering, Appl. Surf. Sci. 188 (2002) 90–96, https://doi.org/PiiS0169-4332(01)00736-X.

[42] V.I. Pinegyn, E.N. Zubarev, V.V. Kondratenko, V.A. Sevryukova, S.A. Yulin, T. Feigl, N. Kaiser, Structure and stressed state of molybdenum layers in Mo/Si multilayers, Thin Solid Films 516 (2008) 2973–2980, https://doi.org/10.1016/j.tsf.2007.10.123.

[43] A.M. Alexander, J.S.J. Hargreaves, C. Mitchell, The denitridation of nitrides of iron, cobalt and rhenium under hydrogen, Top. Catal. 56 (2013) 1963–1969, https://doi.org/10.1007/s11244-013-0133-z.

[44] A.M. Alexander, J.S.J. Hargreaves, C. Mitchell, The reduction of various nitrides under hydrogen: Ni_3N, Cu_3N, Zn_3N_2 and Ta_3N_5, Top. Catal. 55 (2012) 1046–1053, https://doi.org/10.1007/s11244-012-9890-3.

[45] B. Wang, H. Guo, X. Yin, L. Shen, N-sorption capability of Al_2O_3-supported Mn-/Fe-based nitrogen carriers during chemical looping ammonia synthesis technology, Energy Fuels 34 (2020) 10247–10255, https://doi.org/10.1021/acs.energyfuels.0c01000.

[46] S.M. Hunter, D. Mckay, R.J. Smith, J.S.J. Hargreaves, D.H. Gregory, Topotactic nitrogen transfer: structural transformation in cobalt molybdenum nitrides, Chem. Mater. 22 (2010) 2898–2907, https://doi.org/10.1021/cm100208a.

[47] S.M. Hunter, D.H. Gregory, J.S. Hargreaves, M. Richard, D. Duprez, N. Bion, A study of $^{15}N/^{14}N$ isotopic exchange over cobalt molybdenum nitrides, ACS Catal. 3 (2013) 1719–1725, https://doi.org/10.1021/cs400336z.

[48] D.H. Gregory, J.S.J. Hargreaves, S.M. Hunter, On the regeneration of Co_3Mo_3N from Co_6Mo_6N with N_2, Catal. Lett. 141 (2010) 22–26, https://doi.org/10.1007/s10562-010-0464-3.